RSC Advances

ROYAL SOCIETY OF CHEMISTRY

www.rsc.org/advances

Journal Name

RSCPublishing

ARTICLE

Co^{2+}-loaded periodic mesoporous aluminum phosphonates for efficient modified Fenton catalysis†

Cite this: DOI: 10.1039/x0xx00000x

Received 00th January 2012,
Accepted 00th January 2012

DOI: 10.1039/x0xx00000x

www.rsc.org/

Yun-Pei Zhu,[a] Tie-Zhen Ren[b] and Zhong-Yong Yuan*[,a]

Periodic mesoporous aluminum phosphonate (PMAP) materials with homogeneously integrated organophosphonate bridging groups inside the hybrid framework were synthesized by an autoclaving process using ethylene diamine tetra(methylene phosphonic acid) as the coupling molecule, with the assistance of cationic surfactant cetyltrimethylammonium bromide. The prepared aluminum phosphonates possessed high specific surface area of 511 m^2 g^{-1} and a typical hexagonal mesophase, thus guaranteeing the considerable uptake capacity for loading Co^{2+} ions through coordination interaction. The monolayered adsorption behavior of Co^{2+} was confirmed, and the Co^{2+}-loaded PMAP could be further utilized as heterogeneous catalyst for oxidizing decomposition of phenol in the presence of peroxymonosulfate, with favorable kinetic and thermodynamic characteristics. It is suggested that the functionalities of metal phosphonate organic-inorganic hybrids could be rationally designed by judiciously selecting precursors and post-modification, making them potentially applicable in environmental remediation and catalysis.

1. Introduction

Environmental-friendly catalysis is among the most significant applications within the area of nanoscience. Efficient destruction of organic contaminants in the waste water involving advanced oxidation processes (AOPs) has received great scientific and technological interests in environmental applications during last decades.[1-4] AOPs involve the generation of highly active oxidizing species that attack and decompose organic substances, making the oxidizing processes superior over other techniques based on physical processes including adsorption and flocculation. Classical homogeneous Fenton reagent consisting of Fe^{2+} and hydrogen peroxide has been testified to be of valuable degradation efficiency and general applicability, though the requirement of acidic conditions to avoid ferrous and ferric ion hydrolysis and the removal of sludge containing iron ions make this method unamiable and uneconomical.[5,6] Driven by the need of overcoming the drawbacks of Fenton reagent and seeking for another alternative system that can introduce oxidants outperforming the hydroxyl radicals, a variety of modified Fenton systems have been proposed, such as the manganese-, copper-, nickel-based catalysts involving H_2O_2;[7,8] nevertheless, their further application is blocked by the insufficient catalytic performance. Remarkably, among various transition and noble metal ions, Co^{2+} exhibits considerable capability for the activation of peroxymonosulfate (PMS) to produce sulfate radicals, due to the suitable redox potential.[5,9-11] The more powerful oxidizing capability of sulfate radicals than hydroxyl counterparts at neutral pH and their similarity at acidic pH could be related to the abilities of their redox partners as leaving groups, wherein the bisulfate and sulfate ions are for the active sulfate radical and the water molecule for the hydroxyl radical.[12] However, it should be noted that the toxicity associated with cobalt ions during homogeneous reaction leads to further health concern and pollution. On the other hand, recovery and reuse of the catalysts after catalytic reactions are important factors for sustainable process management, while homogeneous Fenton systems are prohibited to a wide application range from this point of view. Moreover, the alleviation of damage from organic contaminants and cobalt ions simultaneously through a facile route remains a challenge.

Heterogenization of the homogeneous catalysts provides a myriad of advantages including ease separation and catalyst reusability. For cobalt-based catalytic systems, several heterogeneous catalysts have been investigated such as Co_3O_4 [13,14] and $CoFeO_4$ nanoparticles,[15] exhibiting obvious Co^{2+}

leaching. Further attempts were made to immobilize the active cobalt species on various supporters, for instance, carbon nanotubes,[16] graphene oxide,[17] activated carbon,[18] magnesium oxide,[19] and titanium oxide.[20] But the corresponding energy–intensive preparation technologies, high cost of the supporting materials and the insufficient catalytic activity subjected to the poor porosity make them find difficulties in the practical applications.

Well-defined mesoporosity accompanied by high specific surface area and large pore volume not only can facilitate interaction between active sites and guest molecules at the pore surface and throughout the bulk of the material, but also promote mass transfer of intermediates, resulting in tremendous potential in the fields of catalysis, adsorption and biotechnology.[21,22] Chemically designed metal phosphonate hybrid mesoporous materials have been proven to be multifunctional due to the combined physicochemical superiorities from inorganic and organic moieties, thereby presenting fantastic surface chemistry for meaningful practicability, and intentional introduction of well-structured mesoporosity by using surfactants could further improve the apparent performances.[23-25] As one of the classical applications, heavy metal ion adsorption for metal phosphonates has attracted wide attention on the basis of that the organic functionalities in the hybrid network typically serve to form complexes with heavy metal ions through acid–base reactions.[21,26] The adsorption behavior of metal ions for the phosphonate-based hybrid adsorbents was found to follow Langmuir-type monolayer model due to the uniform bridging between organic linkages and inorganic units.[26,27] It is reasonable to envision that the toughly immobilized metal ions can act as catalytically active sites for specular reactions, thus achieving the heterogenization of homogeneous catalysts, which is beneficial to the recyclability and reusability of the homogeneous catalytic species. However, there are still scarce reports that realize such an objective.

Herein, periodic mesoporous aluminum phosphonates with high specific surface area were synthesized with the assistance of cetyltrimethylammonium bromide (CTAB) through an autoclaving process, using ethylene diamine tetra(methylene phosphonic acid) (EDTMP) as the organic bridging groups. The homogeneously allocated ethylene diamine functional groups on the mesoporous channels demonstrated high capability to coordinate cobalt ions, realizing the heterogenization of homogeneous active Co^{2+} ions on the hybrid support. A step beyond would be promising in oxidizing decomposition of organic pollutants in the presence of PMS.

2. Experimental

2.1 Chemicals. Aluminium trichloride ($AlCl_3$), cetyltrimethylammonium bromide (CTAB), phenol, and $Co(NO_3)_2$•$6H_2O$ were obtained from Tianjin Guangfu Chemical Co. EDTMP was received from Shandong Taihe Chemical Co., Ltd. Potassium peroxymonosulfate was received from Tianjin Shengmiao Chemical Co. All chemicals were used as received without further purification.

2.2 Synthesis of periodic mesoporous aluminum phosphonate. In a typical run, 1.6 mmol of EDTMP and 2.0 mmol of CTAB were dissolved in the mixed solution of 20 ml of H_2O and 5 ml of ethanol, followed by vigorous stirring for 2 h. Thereafter, $AlCl_3$ was added into the mixed solution very slowly (P/Al molar ratio: 5/4), and the pH value of the mixture was kept around 9.0 through the entire process by ammonia and HCl. Then the homogeneous mixture was transferred into a 50 ml-sized Teflon-lined autoclave and aged statically at 110 ºC under autogenous pressure for 36 h. After cooled naturally to room temperature, the resultant mixtures were filtered and dried. The removal of the surfactant was accomplished by extracting the as-synthesized material in ethanol (200 mL) with concentrated HCl (4.2 g) for 24 h, and the final sample was marked as PMAP. Meanwhile, aluminum phosphonate counterpart with disordered mesoporosity was synthesized through the similar way while in the absence of surfactant, and labeled as MAP.

2.3 Characterization. X-ray diffraction (XRD) patterns were recorded on a Bruker D8 Focus Diffractometer with Cu-Kα radiation (λ = 0.15418 nm) operated at 40 kV and 40 mA. Scanning electron microscopy (SEM) was carried out on a Jeol JSF-7500L microscope at 5 kV. Transmission electron microscopy (TEM) was carried out on a Jeol JEM 2100F microscope at 200 kV. All samples subjected to TEM measurements were ultrasonically dispersed in ethanol and dropcast onto copper grids covered with a carbon film. N_2 adsorption–desorption isotherms were measured on a Quantachrome NOVA 2000e sorption analyzer at liquid nitrogen temperature (77 K). Prior to measurement, the samples were degassed at 120 ºC overnight. Surface areas were calculated by the multi-point Brunauer–Emmett–Teller (BET) method. Fourier transform infrared (FT-IR) spectra were measured on a Bruker VECTOR 22 spectrometer with KBr pellet technique, and the ranges of spectrograms were 4000 to 400 cm^{-1}. X-ray photoelectron spectroscopy (XPS) measurements were performed on a Kratos Axis Ultra DLD (delay line detector) spectrometer equipped with a monochromatic Al-Kα X-ray source (1486.6 eV). All XPS spectra were recorded using an aperture slot of 300 × 700 microns, survey spectra were recorded with a pass energy of 160 eV and high resolution spectra with a pass energy of 40 eV. Thermogravimetry analysis (TGA) was performed using a TA SDT Q600 instrument at a heating rate of 5 ºC min^{-1} using α-Al_2O_3 as the reference. The chemical compositions of Al and P were analyzed by inductively coupled plasma (ICP) emission spectroscopy on a Thermo Jarrell-Ash ICP-9000 (N +M) spectrometer, and C, N, and H were analyzed on a Vario-EL elemental analyzer.

2.4 Metal ion adsorption. The ability of PMAP for Co^{2+} adsorption was tested as follows: 2 mg mL^{-1} of the samples were added into $Co(NO_3)_2$ buffered solution (pH = 6.0, phthalate) with different concentrations of 0.2 to 1.8 × 10^{-4} mol L^{-1}. After stirring for 8 h to access the adsorption–desorption

balance, the mixtures were filtered and the residual metal ion concentrations in the filtrates were analyzed by graphite furnace atomic absorption spectroscopy (AAS). The adsorption capacities of the adsorbent were then determined from the concentration difference measured between the filtrates and the initial metal ion solutions. The maximal adsorption capacity was calculated by the Langmuir model using the equation $n_s = Kn_m c/(1 + Kc)$, where K is the Langmuir constant, c is the Co^{2+} concentration, n_m is the monolayer adsorption capacity, and n_s is the amount of Co^{2+} adsorbed on the adsorbent. The distribution coefficient (K_d) was determined using the equation $K_d = (c_i - c_f)V/(c_f m_{ads})$, where c_i is the initial metal ion concentration, c_f is the ion concentration after adsorption, V is the volume of the solution (in mL), and m_{ads} is the amount of adsorbent (in g).

2.5 Preparation of Co^{2+}@PMAP. The determined monolayer adsorption capacity was considered as the standard for loading Co^{2+} ions. Typically, 1 g of the PMAP sample was added in 10 ml of $Co(NO_3)_2$ buffered solution (pH = 6.0, 1.0×10^{-4} mol L^{-1}) under gentle magnetic stirring for 8 h to achieve the Co^{2+} adsorption saturation. The mixture was filtered, and the resultant Co^{2+}-loaded PMAP material was washed with water and ethanol alternatively to remove excess Co^{2+} ions, and dried at 80 ºC under vacuum conditions for 12 h. The ultimate material was denoted as Co^{2+}@PMAP.

2.6 Catalytic oxidation tests. The catalytic activity of the prepared cobalt phosphonate materials was evaluated by the degradation of phenol with the assistance of PMS. Typically, 20 mg of Co^{2+}@PMAP was added to 50 mL of 10 ppm phenol solution, and the degradation of phenol was initiated using PMS oxidizing agent at a concentration of 6 mmol L^{-1}. Aliquots of reaction solutions were sampled at designated time intervals during the reaction. The absorbance of reaction solutions was measured using a SP-722 spectrometer at λ_{max} = 504 nm. To evaluate the stability of the catalysts, the sample after one trial was collected through centrifugation, washed by water and ethanol alternatively, and dried for the subsequent cycle test.

3. Results and Discussion

3.1 Material synthesis and characterization. Periodic mesoporous aluminum phosphonate material was prepared through a cationic surfactant-assisted sol-gel strategy, wherein $AlCl_3$ was added slowly into the mixed solution of CTAB and EDTMP. The pH value of the reaction system should be kept at around 9.0, which was found to be a crucial factor to obtain well-developed mesostructures. The XRD patterns of the aluminum phosphoantes prepared in the presence of CTAB are shown in **Fig. 1**. The low-angle XRD pattern of PMAP demonstrates a typical hexagonal mesophase with a major diffraction situated at 2θ = 2.08º assigned to (100) reflection, accompanied with two well-resolved peaks at 2θ = 3.65º and 4.16º corresponding to (110) and (200) reflections, respectively. The unit cell parameter (a) was calculated to be 4.9 nm. The periodic mesostructure was further confirmed by TEM and N_2 sorption analysis. The hexagonal arrangement of mesopores

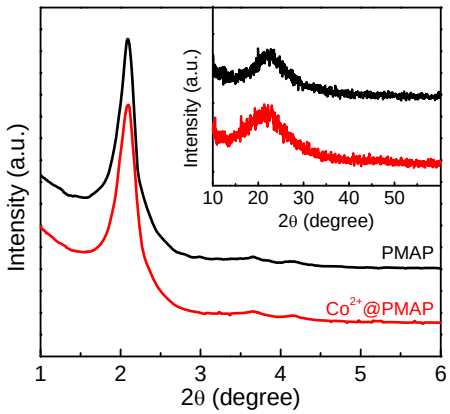

Fig. 1 Low and wide angle XRD patterns of the synthesized PMAP and Co^{2+}@PMAP materials.

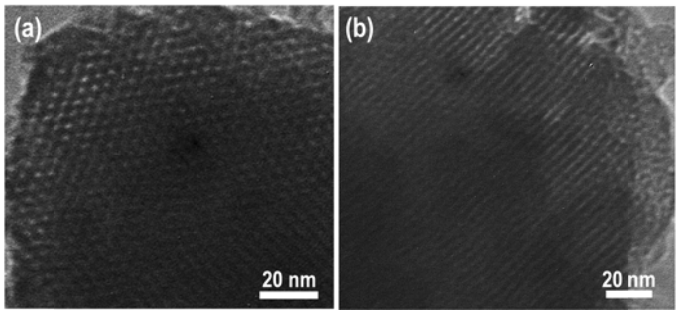

Fig. 2 TEM images of the PMAP sample.

with pore size of about 3.1 nm can be clearly observed in **Fig. 2a**, which is similar to the previously reported aluminum phosphonates prepared with the assistance of CTAB.[28] Moreover, typical one-dimensional channels can be seen from the side view of PMAP (**Fig. 2b**). The N_2 sorption isotherm of PMAP is of type IV without visible hysteresis loop (**Fig. 3**), suggesting reversible capillary condensation-evaporation in mesopores, which is typical for some OOINs (ordered organic-inorganic nanocomposites) with accessible mesostructures.[29] The resulting pore size distribution curve determined by Non-Local Density Functional Theory (NLDFT) model presents a narrow peak around 3.1 nm, coinciding with the TEM observation. The specific surface area and pore volume are calculated to be 511 m^2 g^{-1} and 0.401 cm^3 g^{-1}, respectively. The formation mechanism of the prepared ordered mesoporous aluminum phosphonate hybrid material with the assistance of cationic surfactant CTAB under weakly alkaline condition is proposed that the positive charge-associated CTA^+ micelles and the anionic aluminum phosphonate species were assembled together under the drive of electrostatic and van der Waals interactions, similar to the S^+I^- ionic mechanism.[30,31] This is first example involving the successful ordered mesoporous metal phosphonates under basic conditions to the best of our knowledge.

The skeleton structure and surface chemistry of the mesoporous hybrid were investigated by FT-IR and XPS. The FT-IR spectra of the PMAP sample and coupling molecule EDTMP are shown in **Fig. 4**. The strong broad band at 3400

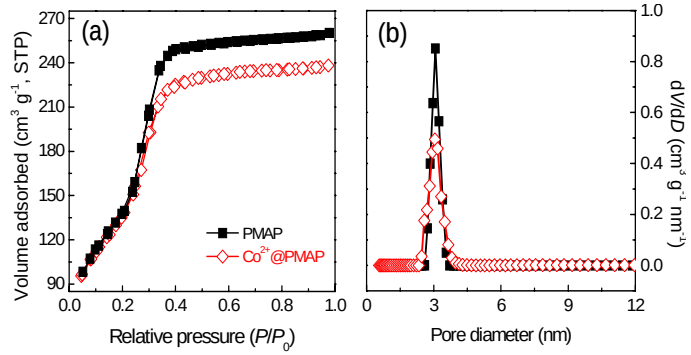

Fig. 3 N_2 adsorption-desorption isotherms (a) of PMAP and Co^{2+}@PMAP, and the corresponding pore size distribution curves (b) determined by the NLDFT model.

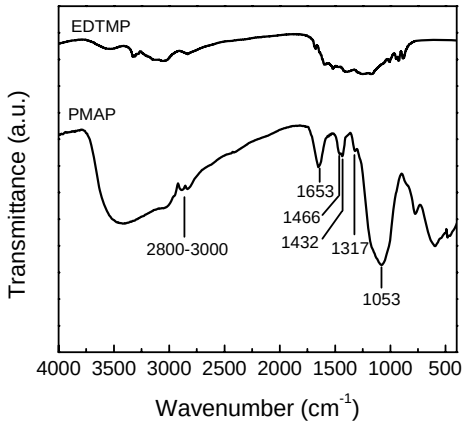

Fig. 4 FT-IR spectra of EDTMP and PMAP.

cm^{-1} and the sharp band at 1653 cm^{-1} correspond to the surface-adsorbed water and hydroxyl groups. The strong band at 1053 cm^{-1} is due to phosphonate P–O–Al stretching vibrations. The overlapped bands at 1466 and 1432 cm^{-1} are assigned as the C–H bending in –CH_2– groups and the P–C stretching vibrations, respectively, and the small band at 1317 cm^{-1} could be attributed to C–N stretching.[32] The signal presented at 740–745 cm^{-1} suggests the presence of P–O–P bending modes. In addition, weak bands around 2800–3000 cm^{-1} are assigned to the C–H stretching modes. The band at 927 cm^{-1} in the spectrum of EDTMP, assigned to P–OH stretching vibrations, is not observed in PMAP, which implies the extensive condensation and coordination of the phosphoryl oxygen with the aluminum atom, leading to mainly bidentate phosphonate units.

High-resolution XPS spectra were also recorded on the surface of the PMAP sample for the investigation of chemical state and surface stoichiometry (**Fig. 5**). The surface atomic composition of the materials was calculated to be 7.48% Al, 9.21% P, 15.62% C, 61.75% O and 4.94% N for PMAP. The surface P/Al ratio was calculated to be 1.23, approximate to 5/4. The Al 2p line of PMAP sample is composed of a single peak situated at binding energy of 74.5 eV (**Fig. S1**, Supplementary Information). Compared with the binding energy of pure Al_2O_3 (75.4 eV for Al 2p),[33] the increase of binding energy for the Al

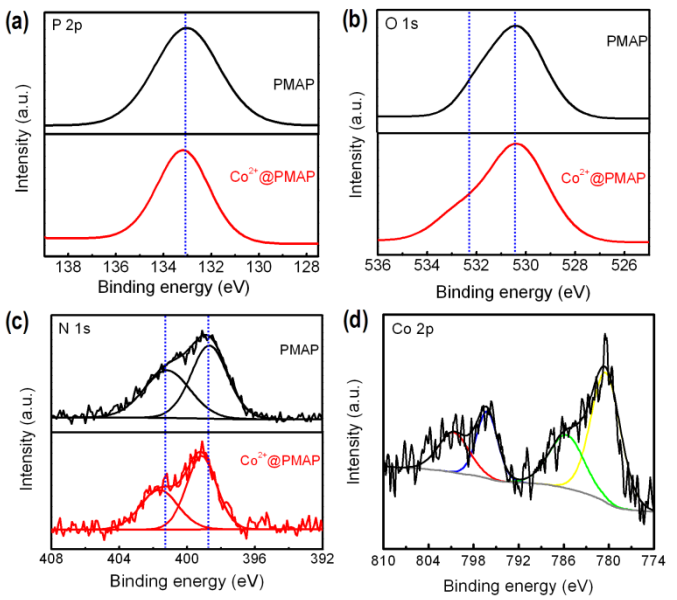

Fig. 5 High-resolution XPS spectra of P 2p (a), O 1s (b) and N 1s (c) for PMAP and Co^{2+}@PMAP, and Co 2p (d) for Co^{2+}@PMAP.

2p in the mesoporous aluminum phosphonate hybrid may be the result from the organophosphonate incorporation in the organic-inorganic network. The P 2p binding energy of PMAP is observed at 131.4 eV (**Fig. 5a**), which is characteristic of P^{5+} in phosphonate groups. In the O 1s spectrum (**Fig. 5b**), the broad signal at 530.3 eV can be attributed to the bridging oxygen in the P–O–Co linkages, and a shoulder around 532.1 eV can be assigned to the surface hydroxyl. The N 1s spectrum (**Fig. 5c**) shows a main component at 398.6 eV with a shoulder at 401.2 eV, attributable to the bridged N-containing compounds.

The thermal stability of the as-synthesized PMAP hybrid material was investigated through thermal gravimetric analysis (TGA). The TGA curves in **Fig. S2** exhibit an initial weight loss of 11.2% from room temperature to 180 ºC, which may be assigned to the desorption of the adsorbed and intercalated water. The second weight loss of 10.1% from 180 to 435 ºC can be attributable to the decomposition of the surfactant molecules, and the third weight loss of 7.3% from 435 to 650 ºC can be associated with the decomposition of the organic functional groups in the hybrid framework. Another small weight loss of 0.5% at beyond 650 ºC can be related to the combustion of carbon species. The TGA characterization showed that the hybrid framework could stay stable up to around 435 ºC, which is also confirmed by previously reported studies concerning mesoporous aluminium organophosphonates.[34,35] The ICP emission spectroscopy was employed to analyze chemical compositions of the resultant solids (13.24% Al, 19.01% P in mass), revealing the P/Al molar ratios approximate to 5:4 in the sample, which was consistent with the ratio of the reagents added, showing the complete condensation of $AlCl_3$ and phosphonic acid. Combined with the conventional elemental analysis of C, H and N (11.04% C, 9.75% H, 4.29% N in mass), the PMAP material could be roughly formulated as $Al_4(EDTMP)_{1.25}$•xH_2O.

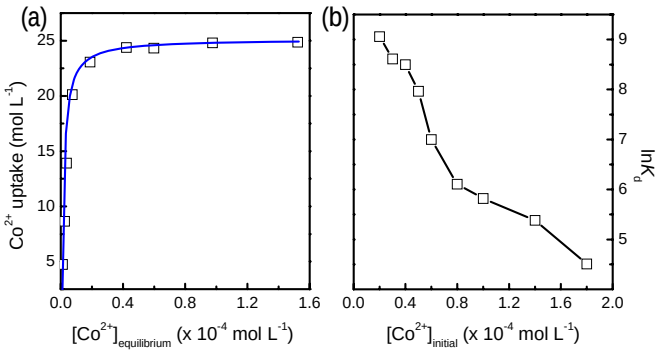

Fig. 6 (a) Co^{2+} ion adsorption isotherm of PMAP, and (b) the corresponding distribution coefficient profile. The solid blue line in (a) is the simulated line using Langmuir equation.

3.2 Co^{2+} ion adsorption. The Co^{2+}-loaded PMAP heterogeneous catalyst was prepared by an adsorption strategy. The Co^{2+} could be immobilized on the hybrid matrix on the basis of coordination effect, and the homogeneously distributed organophosphonate functionalities ensured the high and uniform dispersion on the mesoporous hybrid materials. The Co^{2+} adsorption behavior for the PMAP sample was thus investigated to determine the saturation amount of Co^{2+} ions. The PMAP hybrid was treated with a series of $Co(NO_3)_2$ aqueous solution with different concentrations. It is found that the adsorption behavior follows Langmuir-type model (**Fig. 6a**), with the ions being almost quantitatively adsorbed until binding saturation was reached. According to the Langmuir equation, the maximal adsorption capacity was calculated to be 24.8 μmol g^{-1}, which is set as the standard for loading Co^{2+} ions. As shown in **Fig. 6b**, The PMAP presents high distribution coefficient (K_d) particularly at low Co^{2+} concentrations (8591 ml g^{-1} when treated with 0.2 × 10^{-4} mol L^{-1} Co^{2+} aqueous solution) , which decreases with the increase of the initial concentration. This implies the high affinities for the uptake of Co^{2+} ions at low levels. Noticeably, the resultant adsorption ability outperforms previous reported hierarchically porous titanium phosphonate materials,[36] making the present mesoporous aluminum phosphonates promising adsorbents for the heavy metal ion removal.

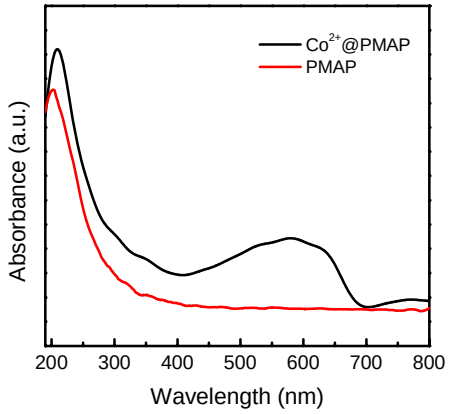

Fig. 7 UV-Vis absorbance spectra of PMAP before and after Co^{2+} ion loading.

The low-angle XRD pattern of Co^{2+}-loaded PMAP (Co^{2+}@PMAP) (**Fig. 1**) exhibits three typical peaks related to hexagonal mesophase, i.e., one main peak corresponding to the (100) reflection and two small peaks assigned to (110) and (200) reflections, suggesting the preservation of the long-range ordered mesostructure after incorporating cobalt ions. The wide angle XRD pattern of Co^{2+}@PMAP presents still the amorphous pore walls. No reflection characteristics of cobalt oxides or hydroxies could be observed. The nitrogen adsorption–desorption isotherms of Co^{2+}@PMAP are of type IV with type H2 hysteresis as well, meaning the reservation of well-defined mesopores. The pore size distribution, obtained from the NLDFT model, present a narrow peak at about 3.1 nm, and the surface area of Co^{2+}@PMAP (506 m^2 g^{-1}) is a little smaller than that of PMAP (511 m^2 g^{-1}), suggesting that the incorporated Co^{2+} ions would not intensively affect the textural and structural properties of the synthesized hybrid material. The TEM images of Co^{2+}@PMAP (**Fig. S3**) also confirmed that the periodic mesoporous structure could be well observed after Co^{2+} loading.

Meanwhile, UV-Vis absorbance spectrum was conducted to illustrate the interaction between Co^{2+} ions and the PMAP host material. **Fig. 7** indicates that absorbance peak of Co^{2+}@PMAP has a red shift from 203 to 210 nm as compared with that of the pristine PMAP. Notably, a broad absorbance shoulder ranging from 400 to 700 nm can clearly be seen. Coordination between Co^{2+} and the pore surface of PMAP is regarded as the reason to the variation of UV-Vis absorbance due to the existence of organophosphonate species in the hybrid network,[26,37] akin to the coordination effect of the ethylenediamine-functionalized porous silica systems.[38,39]

In order to further confirm the chemical nature of Co^{2+} adsorption on PMAP, high-resolution XPS measurements were thus performed. As shown in **Fig. S1** and **Fig. 5**, no obvious differences between PMAP and Co^{2+}@PMAP can be observed in the Al 2p, O 1s and P 2p spectrum. However, after being coordinated with Co^{2+}, the two signals of N 1s corresponding to the bridging nitrogen species in the phosphonic linkages shifted to higher binding energy, which can be due to the formation of the coordination bond of N-metal ions where the electron-rich nitrogen atoms shared electrons with Co and thus electron densities of nitrogen atoms were reduced.[40] For the high-resolution Co 2p spectrum (**Fig. 5d**), the binding energies were observed to be 795.8 eV for Co $2p_{1/2}$ and 780.6 eV for Co $2p_{3/2}$. The spin–orbit splitting value of the 2p peaks was determined to be 14.8 eV, indicating that the immobilized cobalt ions on the mesoporous hybrid wall exist as divalent species.[41] Moreover, relatively intense satellite peaks at 785.7 and 800.8 eV reveal the presence of divalent Co since mixed-valence exhibits a weak satellite structure.[42,43] In fact, the claw tetraphosphonic acid could react with metal ions. The complete chelation between phosphonic acids with aluminum was confirmed by the FT-IR and XPS characterization. Only scare free P-OH ligands were left after the aluminum phosphonate hybrid framework was generated, and thus Co^{2+} adsorption was mainly due to coordination of the N atoms (**Fig. 8**), which was

previously reported for the ethylene–diamine integrated PMOs-based adsorbents.[36,37] The surface atomic composition of Co^{2+}@PMAP was calculated to be 7.45% Al, 9.18% P, 15.66% C, 62.47% O, 4.91% N and 0.33% Co. The surface P/Al ratio was calculated to be 5/4, the same as that of PMAP, implying that no change happened to the chemical compositions and the organic groups in the hybrid framework.

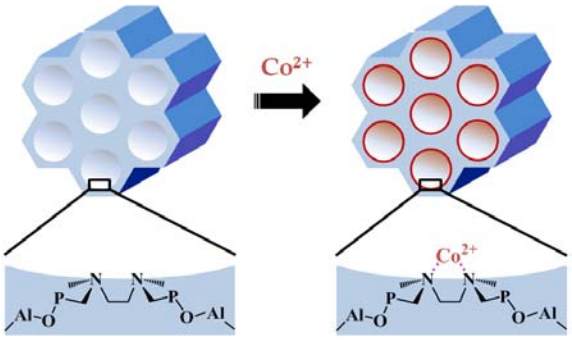

Fig. 8 Schematic illustration of the formation process for the Co^{2+}-loaded PMAP material.

To test the reusability of the PMAP adsorbent, the Co^{2+} ion loaded sample was treated with 1mol L^{-1} hydrochloric acid for 8 h to remove the heavy metal ions and then neutralized, following a second round of metal ion adsorption testing. The results for Co^{2+} adsorption using the regenerated adsorbents are summarized in **Fig. S4**. Only a slight deterioration from 98.6 to 94.3% could be observed during the second use, and the sample retained a Co^{2+} removal efficiency of 92.5% after three cycles. Then the Co^{2+} uptake capacities decreased gradually with the subsequent successive use, but the hybrid still reserved about 85% of the initial metal ion loading capacity after leaching six times. This signifies the stability of the synthesized periodic mesoporous aluminum phosphonate materials and the retention of their adsorption properties under the relatively strong acid leaching conditions, making them useful as reusable sorbents for multiple metal ion adsorption cycles.

3.3 Catalytic performance. The homogeneous Co^{2+}/PMS systems have been testified to be considerably efficient in decomposing organic contaminants.[8-11] The simultaneous incorporation of Co^{2+} and well-defined mesoporosity in the Co^{2+}@PMAP materials inspired us to investigate the catalytic oxidation capability as a Fenton-like heterogeneous catalyst. **Fig. 9a** depicts the variation of phenol concentration as a function of time for different systems. To have a better understanding of the reaction kinetics of the phenol degradation catalyzed by the heterogeneous hybrid catalysts, a general pseudo-first-order kinetics for phenol decay could be assumed: $\ln(C_0/C) = kt$, where C_0/C represents the normalized organic compound concentration and k is the apparent reaction rate constant. As to PMS without a solid catalyst, degradation of phenol is negligible after 60 min, indicating that the PMS itself could not be activated for oxidizing phenol in aqueous solution under ambient conditions. The phenol concentration showed no evident change in the presence of PMAP, which suggested that the consumption of phenol by adsorption process could be ignored. For the PMS/PMAP system, the PMAP material could hardly activate PMS to produce active sulfate species to result in phenol oxidation. Nonetheless, the Co^{2+}@PMAP material could produce significant phenol decomposition with the assistance of PMS, and complete degradation could be achieved within 50 min with the reaction rate constant of 0.0739 min^{-1}. As shown in **Fig. S5**, it can be found that the catalytic efficiency increased with the Co^{2+} loading amount and then reached the maximum after the immobilization ability reached the saturation value. Thus, the mesoporous hybrid materials saturated with Co^{2+} were chosen in the following tests.

In general, the activity of catalyst strongly depends on the properties of support. Here, the ordered mesoporous structures with high specific surface area could contribute to the enhancement of mass transfer and supply abundant sites for loading catalytically active Co^{2+} ions. To confirm this point, the periodic mesoporous structure of Co^{2+}@PMAP was destroyed by a ball-milling treatment, which was denoted as Co^{2+}@d-PMAP, leading to a reduction of surface area to 138 m^2 g^{-1}. Although the resultant materials had the same Co^{2+} loading amount, the oxidizing degradation was decreased to 64.7% after 60 min, accompanied with k = 0.0181 min^{-1}. For the purpose of comparison, mesoporous aluminum phosphonate material with disordered mesostructure (**Fig. S6**), labeled as MAP, was synthesized in a similar way to PMAP while in the absence of cationic surfactant. However, the MAP hybrid possessed a relatively lower surface area of 155 m^2 g^{-1} as compared with that of PMAP (511 m^2 g^{-1}), and the corresponding Co^{2+} uptake capability was determined to be 8.13 μmol g^{-1}. The Co^{2+}@MAP could degrade 53.7% phenol (k = 0.0127 min^{-1}), even exhibiting inferior activity in comparison with that of Co^{2+}@d-PMAP. This could be associated with the distinct Co^{2+} immobilizing amount on these hybrid heterogeneous catalysts.

To identify primary radical species formed during the oxidation decomposition of phenol, quenching experiments were conducted with the addition of specific alcohols. The cobalt-mediated activation of PMS is known to generate three different radicals, hydroxyl, sulfate and PMS.[5,44] It is generally considered that alcohols containing alpha hydrogen, such as ethanol, react at high and comparable rates with hydroxyl and sulfate radicals, and alcohols without alpha hydrogen, including *tert*-butyl alcohol, exhibit high efficiency in quenching hydroxyl radicals but inefficiency in consuming sulfate radicals. However, PMS radicals are relatively inert towards alcohols. According to these properties, the real active radical during the catalytic process can be easily identified through the addition of particular alcohols. **Fig. 9c** demonstrates that the addition of ethanol into the reaction solution results in a remarkable decrease of efficiency to 12.7% after 60 min, indicating that PMS radicals could be excluded from being the primary species. Furthermore, the use of *tert*-butyl alcohol can differentiate the roles of hydroxyl and sulfate radicals. However, the degradation of phenol is slightly affected in the presence of *tert*-butyl alcohol because only about 9% reduction in degradation efficiency is observed after 50 min. This implies

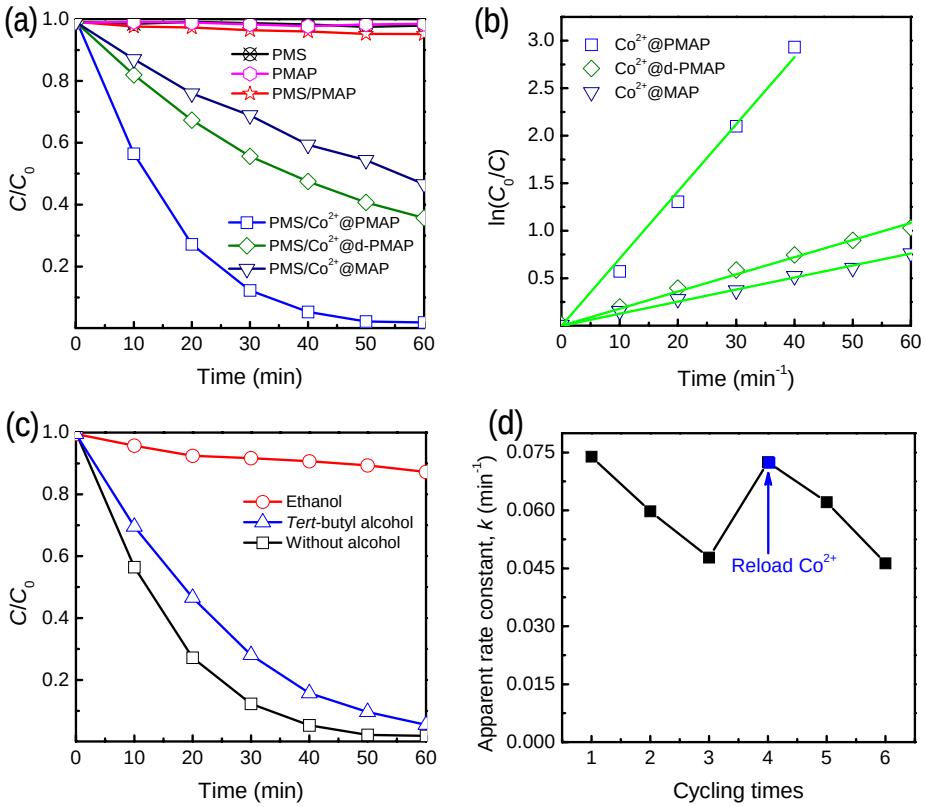

Fig. 9 (a) Degradation kinetic curves of phenol by the synthesized aluminum phosphonate materials as catalysts under ambient conditions, and (b) the corresponding linear fitting results. (c) Quenching studies for radical identification using different alcohols. (d) Reusability tests of Co^{2+}@PMAP for phenol decomposition.

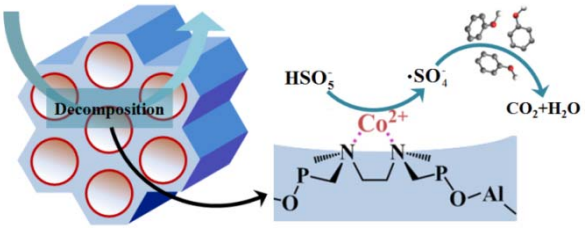

Fig. 10 Scheme of the phenol decomposition process on the pore surface of Co^{2+}@PMAP in the presence of PMS.

that sulfate radicals are the major oxidizing species formed that are indispensable for the transformation of the substrate. The schematic diagram of the oxidation decomposition process is presented in **Fig. 10**.

As the stability of catalytic activity is another parameter to evaluate a heterogeneous catalyst, the catalytic activity of Co^{2+}@PMAP for phenol oxidizing degradation was tested as a reaction time (**Fig. 9d**), where the reactions were carried out under ambient conditions. It is found that the reaction rate of phenol decomposition decreased from 0.0739 to 0.0476 min^{-1} after three times cycling. The analysis of the solution showed that the reaction solution contained 3.2 ppm cobalt ion after the first round and 2.7 ppm cobalt ion leaked in the second run, implying that the loaded cobalt ion was partially leached out after the catalytic reaction. Interestingly, after the Co^{2+} was reloaded onto the repetitiously used Co^{2+}@PMAP, the reloaded Co^{2+}@PMAP almost recovered its catalytic activity. It has been proved that divalent cobalt ion was the best catalyst for activation of PMS because of the suitable redox potential.[5,10] The mechanism of cobalt-based modified Fenton reactions is considered to involve a single electron transfer process, the oxidation of Co(II) with PMS and the formation of sulfate radicals as well as the reduction of Co(III) and the generation of PMS radicals. Quenching experiments testified that the latter transient species were very weak compared to the sulfate ones to induce any degradation of organic pollutants. The active sulfate radicals showed high oxidization ability towards decomposing organics into CO_2, H_2O and other inorganic products. Protonized hydrogen could be generated during the catalysis process, which might cause the Co^{2+} leaching and thus result in the catalytic activity deterioration. In present work, periodic mesoporous aluminm phosphonate hybrid materials with hexagonally aligned mesopores and high specific surface area demonstrate considerable capacity for cobalt ion removal. And the Co^{2+} functionalization endows the mesoporous aluminum phosphonate materials with valuable catalytic activity in the area of environmental remediation.

Reaction temperature is a key factor that influences catalyst activity and phenol removal. Catalytic oxidation reactions were conducted at various temperatures of 25 to 45 ºC to investigate the reaction thermodynamics, as shown in **Fig. 11**. The

degradation rate would increase significantly with the increase of the reaction temperature. According to the first-order kinetic model, the reaction rate constants at different temperatures can be obtained and the relationship is found to follow the Arrhenius equation: $\ln k = \ln A + E_a/RT$, where E_a is the apparent activation energy, R is molar gas constant and T is reaction temperature. The activation energy of Co^{2+}@PMAP for the heterogeneous phenol disintegration is calculated to be 51.8 kJ mol^{-1}, which is lower than most of previously reported supported cobalt-based catalysts in activation of PMS for organic contamitants degradation (Table 1).[18,45-51]

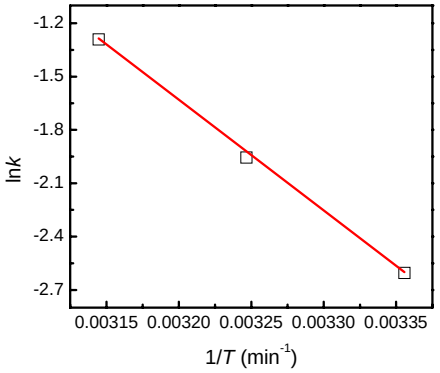

Fig. 11 Effect of reaction temperature on phenol decomposition on the Co^{2+}@PMAP sample.

Table 1. Comparison of the reaction parameters with previously reported cobalt-based catalysts.

Material	Apparent rate constant, k / min^{-1}	Activation energy, E_a / kJ mol^{-1}	Ref.
Co^{2+}@PMAP	0.0739	51.8	This work
Co/activated carbons	0.0827	59.7	18
Co/carbon aerogel	0.0289	62.9	45
Co/SiO_2	–	61.7–75.5	46
Co/ZSM-5	0.000125	69.7	47
Co_3O_4/red mud	0.0428	66.3	48
Co_3O_4/fly ash	0.00513	47.0	48
Co/SBA-15	–	67.4–81.4	49
Co_3O_4/coal ash	0.0111	56.5	50
Co/Fe_2O_3/CS	0.0683	49.5	51

4. Conclusions

Periodic mesoporous aluminum phosphonate hybrid material of hexagonal mesostructure for cobalt ions was prepared through a surfactant-mediated strategy using the nitrogen-contained tetra-phosphonic acid. The homogeneously integrated phosphonate bridging groups in the hybrid framework and large surface area realized the high capability for Co^{2+} ion adsorption. The resultant Co^{2+}-loaded ordered mesoporous hybrid substrates could be further employed as efficient heterogeneous catalysts for oxidizing degradation of organic contaminants with the assistance of peroxymonosulfate. The mesoporous aluminum phosphonates show tremendous potential in the area of sustainable environment development. Furthermore, various metal ions can be immobilized onto the pore wall, and a step beyond including reduction and oxidation makes the organic-inorganic metal phosphonate materials alternative in organic synthesis and photoelectrochemistry.

Acknowledgements

This work was supported by the National Natural Science Foundation of China (21421001 and 21073099), the Program for Innovative Research Team in University (IRT13022), the 111 project (B12015), and the Ph.D. Candidate Research Innovation Fund of Nankai University.

Notes and references

[a] Key Laboratory of Advanced Energy Materials Chemistry (Ministry of Education), Collaborative Innovation Center of Chemical Science and Engineering (Tianjin), College of Chemistry, Nankai University, Tianjin 300071, China.
[b] School of Chemical Engineering and Technology, Hebei University of Technology, Tianjin 300130, China

† Electronic Supplementary Information (ESI) available. See DOI: 10.1039/b000000x/

1 E. Neyens and J. Baeyens, *J. Hazard. Mater.*, 2003, **98**, 33–50.
2 X. J. Long, Z. Yang, H. Wang, M. Chen, K. Y. Peng, Q. F. Zeng and A. H. Xu, *Ind. Eng. Chem. Res.*, 2012, **51**, 11998–12003.
3 S. H. Tian, Y. T. Yu, D. S. Chen, X. Chen and Y. Xiong, *Chem. Eng. J.*, 2011, **169**, 31–37.
4 J. V. Coelho, M. S. Guedes, R. G. Prado, J. Tronto, J. D. Ardissonc, M. C. Pereirad and L. C. A. Oliveir, *Appl. Catal. B*, 2014, **144**, 792–799.
5 G. P. Anipsitakis and D. D. Dionysiou, *Environ. Sci. Technol.*, 2004, **38**, 3705–3712.
6 P. E. F. Oliveira, L. D. Oliveira, J. D. Ardisson and R. M. Lago, *J. Hazard. Mater.*, 2011, **194**, 393–398.
7 C. Yu, G Li, L. Wei, Q. Fan, Q. Shu and J. C. Yu, *Catal. Today*, 2014, **224**, 154–162.
8 A. H. Gemeay, I. A. Mansour, R. G. El-Sharkawy and A. B. Zaki, *J. Mol. Catal. A: Chem.*, 2003, **193**, 109–120.
9 A. Xu, X. Li, S. Ye, G. Yinc, Q. Zeng, *Appl. Catal. B*, 2011, **102**, 37–43.
10 J. Madhavan, P. Maruthamuthu, S. Murugesan, M. Ashokkumar, *Appl. Catal. A*, 2009, **368**, 35–39.
11 T. Warang, N. Patel, R. Fernandes, N. Bazzanella, A. Miotello, *Appl. Catal. B*, 2013, **132–133**, 204–211.
12 S. Steenken, In Free Radicals: Chemistry, Pathology and Medicine; Rice-Evans, C., Dormandy, T., Eds., Richelieu Press: London, 1988, 51–73.
13 G. P. Anipsitakis, E. Stathatos and D. D. Dionysiou, *J. Phys. Chem. B*, 2005, **109**, 13052–13055.
14 X. Y. Chen, J. W. Chen, X. L. Qiao, D. G. Wang and X. Y. Cai, *Appl. Catal. B*, 2008, **80**, 116–121.
15 J. Deng, Y. S. Shao, N. Y. Gao, C. Q. Tan, S. Q. Zhou and X. H. Hua, *J. Hazard. Mater.*, 2013, **262**, 836–844.
16 A. Rodriguez, G. Ovejero, J.L. Sotelo, M. Mestanza and J. Garci, *Ind. Eng. Chem. Res.*, 2010, **49**, 498–505.
17 P. H. Shi, R. J. Su, S. B. Zhu, M. C. Zhu, D. X. Li and S. H. Xu, *J. Hazard. Mater.*, 2012, **229–230**, 331–339.

18 P. R. Shukla, S. B. Wang, H. Q. Sun, H. M. Ang and M. Tade, *Appl. Catal. B*, 2010, **100**, 529–534.
19 W. Zhang, H. L. Tay, S. S. Lim, Y. S. Wang, Z. Y. Zhong and R. Xu, *Appl. Catal. B*, 2010, **95**, 93–99.
20 Q. J, Yang, H. Choi, Y. J. Chen and D. D. Dionysiou, *Appl. Catal. B*, 2008, **77**, 300–307.
21 Y. P. Zhu, T. Z. Ren and Z. Y. Yuan, *New J. Chem.*, 2014, **38**, 1905–1922.
22 Y. P. Zhu, T. Y. Ma, Y. L. Liu, T. Z. Ren and Z. Y. Yuan, *Inorg. Chem. Front.*, 2014, **1**, 360–383.
22 T. Kimura, *J. Nanosci. Nanotechnol.*, 2013, **13**, 2461–2470.
24 T. Y. Ma and Z. Y. Yuan, *ChemSusChem*, 2011, **4**, 1407–1419.
25 J. Wegener, A. Kaltbeitzel, R. Graf, M. Klapper and K. Müllen, *ChemSusChem*, 2014, **7**, 1148–1154.
26 T. Y. Ma, X. Z. Lin and Z. Y. Yuan, *J. Mater. Chem.*, 2010, **20**, 7406–7415.
27 T. Y. Ma, X. Z. Lin and Z. Y. Yuan, *Chem. Eur. J.*, 2010, **16**, 8487–8494.
28 J. E. Haskouri, C. Guillem, J. Latorre, A. Beltrán, D. Beltrán and P. Amorós, *Chem. Mater.*, 2004, **16**, 4359–4372.
29 M. Kruk and M. Jaroniec, *Chem. Mater.*, 2001, **13**, 3169–3183.
30 B. Z. Tian, X. Y. Liu, C. Z. Yu, J. Fan, L. M. Wang, S. H. Xie, G. D. Stucky and D. Y. Zhao, *Nat. Mater.*, 2003, **2**, 159–163.
31 J. E. Haskouri, C. Guillem, J. Latorre, A. Beltrán, D. Beltrán and P. Amorós, *Eur. J. Inorg. Chem.*, 2004, **9**, 1804–1807.
32 A. Dutta, J. Mondal, A. K. Patra and A. Bhaumik, *Chem. Eur. J.*, 2012, **18**, 13372–13378.
33 S. Mathur, M. Veith, H. Shen, S. Hüfner, M. H. Jilavi, *Chem. Mater.*, **2002**, 14, 568–582.
34 T. Kimura, *Chem. Mater.*, 2005, **17**, 337–344.
35 T. Kimura, *Chem. Mater.*, 2005, **17**, 5521–5528.
36 T. Y. Ma, X. Z. Lin, X. J. Zhang and Z. Y. Yuan, *Nanoscale*, 2011, **3**, 1690–1696.
37 T. Y. Ma and Z. Y. Yuan, *Dalton Trans.*, 2010, **39**, 9570–9578.
38 S. Dai, M. C. Burleigh, Y. Shin, C. C. Morrow, C. E. Barnes and Z. Xue, *Angew. Chem., Int. Ed.*, 1999, **38**, 1235–1239.
39 K. Z. Hossain and L. Mercier, *Adv. Mater.*, 2002, **14**, 1053–1056.
40 J. Huang, M. Ye, Y. Qu, L. Chu, R. Chen, Q. He, D. Xu, *J. Colloid Interface Sci.*, 2012, **385**, 137–146.
41 M. M. Natile and A. Glisenti, *Chem. Mater.*, 2002, **14**, 3090–3099.
42 M. M. Natile and A. Glisenti, *Chem. Mater.*, 2005, **17**, 3403–3414.
43 J. Y. Luo, M. Meng, X. Li, X. G. Li, Y. Q. Zha, T. D. Hu, Y. N. Xie and J. Zhang, *J. Catal.*, 2008, **254**, 310–324.
44 H. Liang, H. Sun, A. Patel, P. Shukla, Z. H. Zhu and S. Wang, *Appl. Catal. B*, 2014, **127**, 330–335.
45 Y. Hardjonoa, H. Q. Sun, H. Y. Tian, C. E. Buckley, S. B. Wang, *Chem. Eng. J.*, 2011, **174**, 376–382.
46 P. Shukla, H. Q. Sun, S. B. Wang, H. M. Ang, M. O. Tade, *Sep. Purif. Technol.*, 2011, **77**, 230–236.
47 P. Shukla, S. Wang, K. Singh, H. M. Ang, M. O. Tadé, *Appl. Catal. B*, 2010, **99**, 163−169.
48 E. Saputraa, S. Muhammada, H. Sun, H. M. Ang, M. O. Tadé and S. Wang, *Catal. Today*, 2012, **190**, 68−72.
49 P. Shukla, H. Sun, S. Wang, H. M. Ang and M. O. Tadé, *Catal. Today*, 2011, **175**, 380−385.
50 S. Muhammad, E. Saputra, H. Sun, J. C. Izidoro, D. A. Fungaro, H. M. Ang, M. O. Tadé and S. Wang, *RSC Adv.*, 2012, **2**, 5645–5650.
51 Y. Wang, H. Sun, H. M. Ang, M. O. Tadé and S. Wang, *Chem. Eng. J.*, 2014, **245**, 1– 9.